Contents lists available at *Dergipark*

Journal of Scientific Reports-A

journal homepage: *https://dergipark.org.tr/tr/pub/jsr-a*

E-ISSN: 2687-6167 ***Number 60, March 2025***

RESEARCH ARTICLE

Receive Date: 06.01.2025 *Accepted Date: 14.02.2025*

Determining alternative patch sizes for rectangular microstrip antennas using DE and PSO algorithms

Bahadır Hiçdurmaz[a]*

[a] *Department of Electrical and Electronics Engineering, Kütahya Dumlupınar University,Kütahya, Türkiye, ORCID:0000-0002-4610-1400*

Abstract

With the rapid development of mobile devices, designing microstrip antennas with various patch dimensions and shapes for the same resonant frequency f_r has become increasingly important for better performance and compact design. This study introduces an original theoretical approach for the analysis and design of conventional rectangular patch microstrip antennas (RPMAs). The proposed method focuses on individually optimizing the dimensions of the patch using the differential evolution (DE) algorithm and the particle swarm optimization (PSO) algorithm to estimate f_r of conventional RPMAs. Alternative solutions are presented at f_r of 6.2 GHz for the specified search spaces of the patch dimensions using both the DE and PSO algorithms. The performance of both algorithms is evaluated comparatively over 30 runs. Additionally, the results obtained from the optimization algorithms are validated using the method of moments (MoM) -based IE3D software program, where the position of the probe feed is optimized. The best S_{11} performance achieved from the optimizations for the 6.2 GHz resonant frequency is an S_{11} value of -50.28 dB, with a -10 dB impedance bandwidth of 280 MHz. Furthermore, the validity of the IE3D program is tested against the resonant frequencies of some RPMAs determined experimentally from the literature, demonstrating relatively good agreement.

Keywords: Rectangular patch microstrip antenna; Differential evolution algorithm; Particle swarm optimization algorithm; IE3D; Alternative patch sizes; Resonant frequency.

* Corresponding author. Phone number: +90-5445818684
E-mail address: bahadir.hicdurmaz@dpu.edu.tr.

1. Introduction

Microstrip antennas [1-7], also known as patch antennas, continue to enjoy great popularity in industrial and commercial applications due to their uncomplicated design features. Their wide use extends to areas such as medical, military, and wireless communications, capitalizing on their advantages in terms of simple design, robustness, lightness, and ease of manufacture. The design of a microstrip antenna involves determining the physical dimensions based on the chosen substrate material and operating frequency. The performance of the antenna is then evaluated by calculating and measuring properties such as f_r, bandwidth (*BW*), input impedance and radiation patterns of the *E* and *H* planes as well as the beamwidth. Various patch shapes are used to design microstrip antennas, with square, rectangular, dipole (strip) and circular shapes being among the most commonly used. These shapes are preferred because of their simplicity in analysis, ease of manufacture and attractive radiation characteristics, especially low cross-polarisation. Microstrip antennas can be fed with different configurations, including microstrip line, probe feed, aperture coupling, and proximity coupling, which allows for flexible application and integration into different systems. Thanks to these properties, these antennas are still the subject of academic and commercial research today.

RPMAs are among the most commonly used antennas and are characterized by the length and width of the patch. Like most standard patch microstrip antennas, conventional RPMAs typically have a narrow bandwidth. Therefore, accurately estimating the resonant frequencies of these antennas and determining the size of their patches is crucial for applications that require high frequency selectivity. The literature contains numerous studies [3-32] and more that have been conducted for this purpose. Some of these studies aim to derive empirical or closed-form formulas to calculate f_r or the edge extension length ΔL based on the experimental results, while some others focus on estimating the dimensions or ΔL for the desired f_r using optimization algorithms [6-31]. ΔL was first introduced by [32] to account for the fringing field effect of the patch. Later, the expression for calculating f_r of the rectangular microstrip antenna, based on ΔL was provided by [6]. Immediately afterwards, [7] proposed a different expression for f_r using a modified ΔL. Then, an approximate expression for calculating f_r of rectangular patch antennas was derived from [8]. In the meantime, [9] have found a much more accurate expression for ΔL, which gives a much more precise result for f_r even for a substrate with an electrical thickness of 0.229. In addition, artificial neural networks (ANN) [10] and optimization algorithms such as the Taguchi method [11], the Levenberg-Marquardt algorithm [12], the simplex search method [13], and the differential evolution (DE) algorithm [14] were used to obtain new expressions for ΔL. In [15], rectangular microstrip antennas with different electrical thicknesses of around 0.03 to 0.23 were investigated experimentally, and their resonant frequencies were measured and compared with the existing formulae. When comparing the measurement results with the theories of [7] and [32] it was found that the predicted resonant frequencies for electrically thin substrates closely matched the measured resonant frequencies. However, with increasing electrical thickness, [7]'s estimated values approached the real values by 4% less, while [32]'s estimated values approached them by 8% more. The study in [16] introduces a new expression for the fringe effect of electrically thick rectangular microstrip antennas. The newly derived closed-form expressions for the prediction of f_r showed excellent agreement with the experimental results available in the literature. [17] has presented a new antenna model and a new formula for calculating f_r of electrically thick rectangular microstrip patch antennas. In the study of [18], formulas based on transmission line, cavity, and magnetic wall models were analyzed to determine the resonant frequencies of rectangular microstrip antenna elements, and their validity was evaluated. The antennas were implemented with different variations of the antenna parameters and the experimental results were compared with the theoretical predictions. It has been established that the formulae are valid subject to certain restrictions. In [19], three closed-form formulae were given for calculating the resonant frequencies of rectangular microstrip antenna elements. The calculated results were compared with the measured resonant frequencies of antennas with certain parameters. It was found that the calculated results corresponded well with the measured results. In [20], formulae were derived experimentally to determine the physical properties of the antenna and the effective dielectric constant. In addition, this study has provided an approach for predicting the feed points of the antennas using curve-fitting methods. The study of [21] evaluated the suitability and applicability thresholds of the formulae available in the literature for the

design of the physical properties of rectangular microstrip antennas. New formulae for determining the physical properties of antennas were also determined empirically. In the study of [22], the effects of mechanical tolerances, surface waves, dielectric, radiation and conductor losses, the thickness, dimensions and permeability of the substrate material, the dimensions of the patch, the position of the feed point and the size of the ground plane were investigated. In [24], genetic algorithm (GA) was used to calculate the optimized length and width of electrically thin rectangular microstrip antennas. The IE3D software and experimental results from the literature were used to validate GA's prediction. It was found that the results were in good agreement. In [25], new simple closed-form formulas for calculating the patch length and width of electrically thin and thick rectangular microstrip antennas were established using curve-fitting techniques. It was found that the theoretical results obtained are in very good agreement with the available experimental results in the literature. In [26], a new closed-form expression for the prediction of f_r of a rectangular microstrip antenna was determined using the differential evolution (DE) method for edge extension. The validity of the expression was confirmed with experimental results from 46 different antennas in the literature and with results from other theoretical expressions. An average deviation of 0.7% from the experimental results was obtained. In [27], closed-form formulas were developed using DE algorithm to determine the patch dimensions of electrically thin and thick rectangular microstrip antennas. The results of these proposed closed-form formulas were compared with theoretical and experimental results obtained from 33 antennas studied previously, revealing that the results obtained from the proposed formulas were closer to the experimental results. In [28], particle swarm optimization was utilized to calculate the optimized length and width of rectangular microstrip antennas. The results obtained were found to be consistent with experimental and other metaheuristic methods reported in the literature. In [29], the physical and material parameters of rectangular patch microstrip antennas were predicted using an ANN model for their resonant frequencies. In [30], surrogate model (SM)-based methods were proposed for the design of rectangular microstrip antennas with respect to their f_r and bandwidth. In [31], selective neural network ensemble (NNE) methods based on decimal PSO and binary PSO were proposed to design rectangular patch microstrip antennas according to their f_r.

The evolution of microstrip antennas over the past few decades has been substantial, resulting in designs with increasingly complex structures. Despite the abundance of microstrip antenna designs featuring various patch shapes customized for different purposes and efforts to enhance design processes in the literature, some of which are provided in [33-43], microstrip antennas with standard patch shapes continue to persist in modern applications. Additionally, standard patch microstrip antennas form the foundation for most complex designs.

Recently, metaheuristic algorithms [44] have been increasingly employed to solve complex problems that prove challenging or even impossible to solve using conventional numerical methods. In the existing literature, several algorithms have been developed for such problem-solving scenarios. The main algorithms in this category include GA, PSO, DE, artificial bee colony (ABC), ant colony optimization (ACO), harmony search (HS), loaded system search (CSS), and gravitational search algorithm (GSA). Among these algorithms, DE [45-52] and PSO [53-61] have become popular in electromagnetic and antenna design applications in recent years. They are powerful and valuable algorithms that can be implemented with simple code.

In light of the relevant literature, we believe that no study has been conducted so far on determining alternative patch sizes for conventional RPMAs designed to operate at a specific f_r. Therefore, this work proposes a novel approach model utilizing either the DE or PSO algorithm to design multiple RPMAs for the same specified f_r. Essentially, this study performs a 3D space search to comprehensively explore the solution space and identify the optimal configurations for the given problem. DE and PSO algorithms have been separately applied to calculate the various patch dimensions of conventional RPMAs operating at a f_r of 6.2 GHz for Wi-Fi applications. Additionally, the performances of the DE and PSO algorithms for this problem have been statistically analyzed. The study also explores finding different rectangular patch dimensions for the desired f_r through the graphical method. However, achieving the exact desired f_r using this approach proves more challenging compared to the precision obtained through optimization algorithms. Obtaining different rectangular patch dimensions for the desired f_r is important for providing design flexibility for various applications. The proposed model in this study demonstrates that the patch dimensions

of the conventional RPMA will not be unique for a specific f_r. Furthermore, the accuracy of the study has been verified using the IE3D program. Finally, the validity of the methods used in the study has been compared with measured results for different resonant frequencies found in the literature, and it has been observed that the results are sufficiently consistent.

The organization of the paper is as follows: Section 2 introduces the theoretical background of a conventional RPMA. In Section 3, the classical DE and PSO algorithms are introduced, respectively. In Section 4, the application of the DE and PSO algorithms to the problem is discussed. Section 5 presents and interprets the simulation results obtained. Finally, Section 6 concludes the article by assessing the study and its findings.

2. Conventional RPMA Theory

For a conventional RPMA, the parameters include the length L and the width W of the patch, the substrate thickness h, the dielectric constant ε_r of the substrate, and the feed point location x_{in}, as depicted in Figure 1.

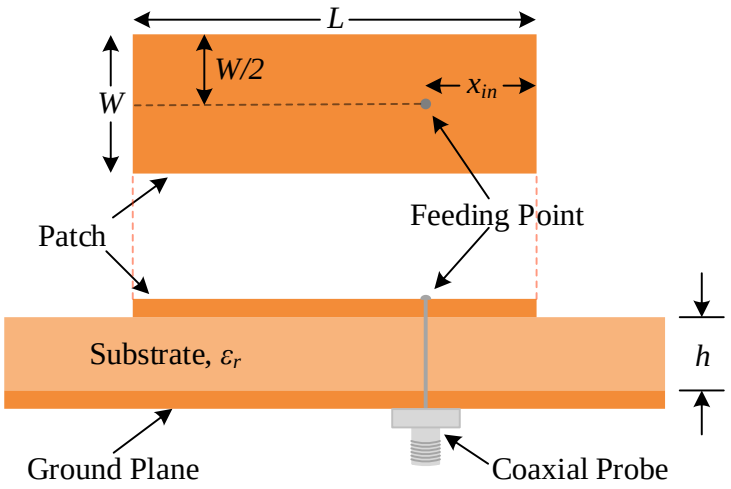

Fig. 1. RPMA with probe feeding.

The resonant frequency of RPMA with the fringing effect can be estimated as [1, 2, 5]

$$f_r = \frac{c}{2\left(L+\Delta L\right)\sqrt{\varepsilon_{eff}}} \tag{1}$$

where $c \approx 3\times10^8$ m/s is the velocity of the electromagnetic waves in free space and ε_{eff} is the effective dielectric constant for substrate with dielectric constant, ε_r, which is expressed by [32]

$$\varepsilon_{eff} = \frac{\varepsilon_r+1}{2} + \frac{\varepsilon_r-1}{2\sqrt{1+12h/W}} \quad \text{for } \frac{W}{h}>1 \tag{2}$$

and ΔL is the edge extension length and is given by

$$\Delta L=0.412\,h\,\frac{\left(\varepsilon_{eff}+0.3\right)\left(\frac{W}{h}+0.264\right)}{\left(\varepsilon_{eff}-0.258\right)\left(\frac{W}{h}+0.813\right)} \tag{3}$$

For a rectangular patch, the length, L of the patch is usually $0.3\lambda_0 < L < 0.5\lambda_0$, where λ_0 is the free-space wavelength. The substrate thickness h is usually $0.003\lambda_0 \leq h \leq 0.05\lambda_0$. The dielectric constant of the substrate (ε_r) is typically in the range of $2.2 \leq \varepsilon_r \leq 12$. For thin substrates, the empirical approximation of the patch width W presented by [6] is given as

$$W=\frac{\lambda_0}{2\sqrt{0.5\left(\varepsilon_r+1\right)}} \tag{4}$$

W is typically the first parameter to be selected in the design process. In this study, the L and W parameters of the patch are determined using equations (1) to (3).

3. Algorithms of the study

In this section, the general explanation of classical DE and PSO algorithms used to obtain alternative sizes in certain search spaces of RPMAs that will operate at a certain resonant frequency is discussed respectively.

3.1. Differential evolution algorithm

DE [44], a widely adopted algorithm in scientific and engineering circles, emerges as a potent population-based evolutionary approach for optimizing continuous variables across multidimensional domains. The basis of the algorithm is to obtain a new solution by subjecting the chromosomes, each of which contains a solution, to individual operators. At its core, the algorithm operates by subjecting chromosomes, each representing a solution, to specific operators in order to generate new solutions. During these operations, mutation and crossover operators are employed. If the newly generated individual exhibits superior fitness, indicating its proximity to the solution, it replaces the old individual in the subsequent population; otherwise, the old individual persists into the next generation. The fundamental parameters employed in DE encompass population size (NP), variable dimensionality (D), maximum iteration count (g_{max}), scaling factor (F), and crossover ratio (CR). The algorithm unfolds through several steps, including variable assignment and initial population generation, individual fitness computation, selection, mutation, crossover, and ultimately, halting the algorithm. In DE, a minimum of three chromosomes is essential to generate a new individual. Hence, the designated population size must exceed three ($NP > 3$). The initial population is formed based on equation (5).

$$\forall p \leq D \cap \forall q \leq NP: \qquad X_{p,q,g=0} = X_p^{min} + r_{p,q,g}[0,1]\times\left(X_p^{max} - X_p^{min}\right) \tag{5}$$

Here, the parameter $X_{p,q,g}$ represents the p^{th} gene of the q chromosome in the g^{th} generation, while X_p^{min} and X_p^{max} represent the lower and upper limits of the genes, respectively. $r_{p,q,g}[0,1]$ signifies a uniformly distributed random number ranging from 0 to 1.

The mutation process entails introducing random alterations to the genes of a chromosome. During this process, three additional chromosomes, denoted as r_1, r_2, and r_3, are chosen alongside the target chromosome for mutation.

Firstly, the disparity between the selected chromosomes r_1 and r_2 is computed, and subsequently, it is multiplied by a designated scaling factor F. Following this, the resultant weighted difference chromosome is merged with the chosen r_3 chromosome. The expression for the intermediate chromosome $N_{q,g}$ essential for the mutation process is depicted in equation (6).

$$\forall p \le D: \quad N_{p,q,g} = X_{p,r_3,g} + F \cdot (X_{p,r_1,g} - X_{p,r_2,g}) \tag{6}$$

The scaling factor F serves as a parameter dictating the pace at which the population evolves in DE. Typically, in the literature, a value within the range of [0, 1] is commonly employed for the scaling factor F. This value plays a pivotal role in dictating the pace at which the population evolves throughout the optimization process.

During crossover, the trial chromosome $U_{p,g}$ is generated utilizing the intermediate chromosome $N_{p,g}$ obtained from mutation and the target chromosome $X_{p,g}$. The genes of this novel chromosome are chosen from the intermediate chromosome with a probability of CR and from the target chromosome with a probability of $1-CR$. The condition $q=q_{\text{rand}}$ is utilized to ensure that at least one gene is inherited from the intermediate chromosome. The resulting new chromosome arising from crossover is defined by

$$\forall p \le D: \quad U_{p,q,g} = \begin{cases} N_{p,q,g} & if \ r_{p,q,g}[0,1] \le CR \cup p = p_{rand} \\ X_{p,q,g} & otherwise \end{cases} \tag{7}$$

The criterion for determining whether the target chromosome or the trial chromosome will be propagated to the next generation hinges on their respective fitness values. Whereas the fitness value of the target chromosome is already known, the fitness value of the freshly created trial chromosome must be computed. Indeed, this computation entails assessing the performance of the trial chromosome with respect to the objective function of the optimization problem. The objective function serves to quantify the merit of a candidate solution based on predefined criteria or constraints. By subjecting the candidate solution represented by the trial chromosome to the objective function, its fitness value is ascertained.

Once the fitness values of both the target and trial chromosomes are computed, the DE algorithm juxtaposes them to determine which chromosome to incorporate into the subsequent generation. Generally, if the fitness value of the trial chromosome surpasses (e.g., lower for minimization problems or higher for maximization problems) that of the target chromosome, the trial chromosome supplants the target chromosome in the population. Conversely, if the trial chromosome's fitness value is inferior, the target chromosome persists in the population for the next generation.

Chromosomes with higher fitness are selected for advancement to the next generation. In optimization aimed at minimization, the expression for the selection process is provided in (8).

$$\forall q \le NP: \quad X_{q,g+1} = \begin{cases} U_{q,g} & if \ f_q(U_{q,g}) \le f_q(X_{q,g}) \\ X_{q,g} & otherwise \end{cases} \tag{8}$$

Here, $f(x)$ represents the objective function that we endeavor to optimize. This cyclic process persists until $g=g_{max}$. Upon reaching $g=g_{max}$, the best available individual is regarded as the solution. g_{max} signifies the predetermined maximum iteration count to conclude the algorithm.

3.2. Particle swarm optimization algorithm

The classical PSO algorithm [52] is inspired by the collective behavior observed in natural communities, such as

ant colonies, bee swarms, bird flocks, or fish schools. Within this framework, the term "particle" refers to an individual entity in the collective, such as a bee in a colony or a bird in a flock. Each particle in the PSO algorithm represents a potential solution to the optimization problem. A particle is characterized by two key attributes: its position and its velocity. In the PSO algorithm formulation, each particle is initialized with random positions, as shown in equation (4), similar to the initialization process in the Differential Evolution (DE) algorithm. Here, $X_{p,q,g}$ denotes the initial position of particle q for variable p, while X_p^{min} and X_p^{max} represent the lower and upper bounds of the position range, respectively. The term $r_{p,q,g}[0,1]$ is a uniformly distributed random number between 0 and 1 for particle q of variable p at the initial position. The new velocity and position of each particle are updated iteratively using specific mathematical formulations. These updates are governed by equations (9) and (10), respectively, as cited in [54, 58, 59].

$$v_{p,q}(t+1) = w(t)v_{p,q}(t) + c_1 r_{1p}(t)\left(P_{\text{best},p,q}(t) - X_{p,q}(t)\right) + c_2 r_{2p}[G_{\text{best},p}(t) - X_{p,q}(t)] \tag{9}$$

$$X_{p,q}(t+1) = X_{p,q}(t) + v_{p,q}(t+1), \qquad \forall q = 1,2,...,NP \tag{10}$$

where t is the current iteration number; NP is the total number of particles in the swarm at each iteration; $X_{p,q}(t)$ is the position of the q^{th} particle for the p^{th} variable at iteration t; $v_{p,q}(t)$ is the velocity of the q^{th} particle for the p^{th} variable in iteration t; positive numbers c_1 and c_2 are positive acceleration constants, also known as the cognitive and social learning factors, respectively; $r_{1p}(t)$ and $r_{2p}(t)$ are random numbers uniformly distributed in the range [0, 1] for the p^{th} variable at iteration t, and $w(t)$ is the inertia weight factor at iteration t. Additionally, within each iteration t, the best position of any particle in the swarm, stored in their own memories, is recorded in the variable $P_{\text{best},p,q}(t)$. The best position among the particles closest to the optimum in the swarm is stored in the variable $G_{\text{best},p}(t)$.

Indeed, the inertial weighting factor $w(t)$ plays a crucial role in balancing the global search ability and local search ability of the PSO algorithm. In the literature, diverse suggestions are provided for adjusting the inertia weight, tailored to the specific problem at hand. Adjusting the inertia weight appropriately is vital for achieving an effective balance between exploration and exploitation during the optimization process. Initially, [53] introduced the inertia weight as a constant value within the range of [0.8, 1.2] for each iteration. Another proposal [54, 58, 59] suggests that the inertia weight, calculated according to equation (11), linearly decreases with each iteration t.

$$w(t) = w_{max} - t\left(\frac{w_{max} - w_{min}}{t_{max}}\right) \tag{11}$$

In equation (11), w_{max} and w_{min} denote the starting and ending inertial weighting factors, respectively, while t_{max} corresponds to the maximum number of iterations, determining the total runtime of the optimization process. Additional critical parameters include the velocity limits [V_{min}, V_{max}], which constrain the velocity of particles to prevent excessively large jumps, thereby ensuring a controlled and efficient search process. Similarly, the particle position limits [X_{min}, X_{max}] guarantee that particles remain within the predefined solution space, avoiding invalid regions during the optimization [58].

4. Applications of DE and PSO algorithms to the problem

In this section, the optimization of the patch dimensions concerning f_r is presented separately using both DE and PSO. The cost function, denoted as CF, for the given problem is succinctly defined in equation (12).

$$CF = minimize\left\{ \left| \Delta f_{r_{opt}} \right| \right\} \tag{12}$$

where $\Delta f_{r_{opt}}$ is expressed by (13).

$$\Delta f_{r_{opt}} = \left(1 - \frac{f_r}{f_{rdes}} \right) \tag{13}$$

where f_{rdes} is the desired f_r. Consequently, the problem is formulated as a cost minimization problem.

At the outset, the population, consisting of *NP* sets of patch length *L* and width *W* values is randomly generated using equation (5). In this equation, $X_{p,q}^{min}$ and $X_{p,q}^{max}$ are the lower (L_{min} , W_{min}) and upper (L_{max} , W_{max}) limits of the length *L* and the width *W* of the patch, respectively. Then, utilizing (1) to (3), f_r values of RPMA are determined for *NP* individuals in DE or *NP* particles in PSO, and the minimum ones are identified (local bests). From these minima, individual or particle with the lowest value is identified along with its corresponding value (global best). Consequently, the optimal *L* and *W* values of the initial generation, along with the associated best f_r values, are obtained. Subsequently, the process transitions to the next generation (iteration 1). This process remains consistent for both DE and PSO algorithms.

From this point onward, the solution to the problem with DE proceeds as follows: Initially, the *F* and *CR* values for DE are specified. Subsequently, the mutation, crossover, and selection processes are executed sequentially using (6), (7), and (8), respectively. This iterative process persists until the maximum iteration value is reached. Resonant frequency obtained at the maximum iteration represents the value closest to the desired f_r.

The solution to the problem with PSO unfolds as follows: Initially, the PSO parameters, including c_1, c_2, V_{min}, V_{max}, w_{min}, and w_{max} values, are defined. In the subsequent generation (iteration 1), the new velocities and positions of each particle are calculated using equations (9) and (10), respectively. It's ensured that the velocities of the particles remain within the specified minimum and maximum velocity range [V_{min}, V_{max}]. Additionally, the particles' positions, which correspond to the *L* and *W* values of the patch, must be within the specified range [X_{min}, X_{max}]. Then, equations (1) to (3) are employed to calculate f_r values of RPMA for *NP* particles, and the minimum for each particle is identified as the local best. The recently acquired local bests are then contrasted with the previous ones. If the new value surpasses the previous local best, it becomes the new best; if not, the previous local best is retained. Subsequently, the particle with the minimum value among these local bests, along with its corresponding value (global best), is determined. This process provides the optimal length *L* and width *W* of the initial generation, along with the corresponding best f_r values. These procedures are repeated until the predetermined number of iterations is reached, with the f_r value from the last iteration representing the best solution.

The flowchart illustrating the solution process with DE or PSO is presented in Figure 2. Table 1 presents the DE and PSO parameters used for optimizing the problem. These parameter values are widely reported in the literature and have been validated for their effectiveness in addressing this specific issue.

To evaluate the practical validity of this study, the obtained results were compared with measurement results reported in the literature for standard rectangular microstrip antennas. The deviation of the obtained results from the measured results is determined by the following expression.

$$\Delta f_r = 100\% \left(1 - \frac{f_{rc}}{f_{rm}} \right) \tag{14}$$

where f_{rc} and f_{rm} are the calculated and measured resonant frequencies, respectively.

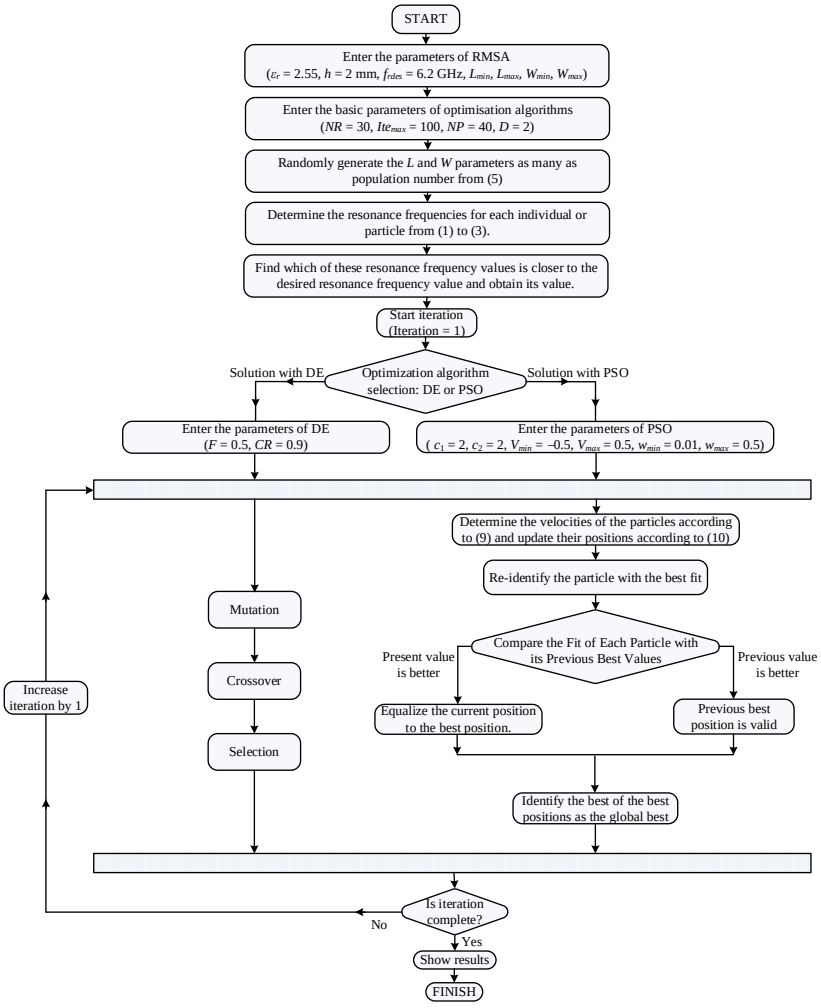

Fig. 2. Flowchart for solving the problem using either DE or PSO.

Table 1. DE and PSO parameters.

Common parameters for DE and PSO	
Gene bounds for DE or particle position bounds for PSO, [X_{min}, X_{max}]	[(L_{min}, W_{min}), (L_{max}, W_{max})]
Maximum iteration number, $g_{\max}$ for DE or $t_{\max}$ for PSO	100
Number of population, NP	40
Number of run, NR	30
The parameters of DE	
Scaling factor, F	0.5
Crossover ratio, CR	0.9
The parameters of PSO	
Learning factor, c_1	2

Learning factor, c_2	2
Velocity bounds, [V_{min}, V_{max}]	[-0.5, 0.5]
Maximum number of iteration, t_{max}	250
Starting and ending inertial weights, [w_{max}, w_{min}]	[0.5, 0.01]

5. Results

To analytically visualize possible patch sizes at a certain f_r, e.g. 6.2 GHz, where ε_r = 2.55 and h = 2 mm of the substrate, a diagram is shown in Figure 3, which shows the variation of f_r in relation to the width of the patch (W) and the length of the patch (L). All five possible sizes are shown here, indicating a variety of designs for this f_r. Then, for f_{rdes} = 6.2 GHz, the dimension values in the search spaces (L_{min}, L_{max}) and (W_{min}, W_{max}) were determined separately with DE and PSO. Both algorithms were run 30 times, and the best solutions were selected from these runs. To demonstrate the accuracy of the study, the IE3D program was used to design microstrip antennas. Using the L and W values determined by DE and PSO, the position of the probe feed (x_{in}) was optimized using IE3D's adaptive EM optimizer to achieve the minimum S_{11} value at the 6.2 GHz frequency. f_r and -10 dB BW were determined from the resulting frequency response curve of S_{11}. The results obtained with DE and PSO are shown in Tables 2 and 3, respectively. The tables show that the best solutions with zero cost are obtained for the same thirteen search spaces in both algorithms. However, when IE3D uses the patch sizes obtained from these solutions, some slight deviations from f_r of 6.2 GHz are observed. Among the patch sizes obtained with DE, the best impedance-matched RPMA patch size obtained with IE3D has a patch size of L = 13.99 mm and W = 19.29 mm, while among the patch sizes obtained with PSO, the best impedance-matched RPMA patch size obtained with IE3D has a patch size of L = 13.98 mm and W = 19.70 mm. These antennas are highlighted in bold in the tables. Eight different patch sizes were determined within the same search space (0, 20) mm for both L and W of DE and PSO. Possible patch sizes for the desired f_r can be taken from Figure 3. However, predicting these quantities using metaheuristic algorithms is a faster, simpler, more practical and more precise approach. In order to achieve a f_r of exactly 6.2 GHz with IE3D while keeping the values for the W length constant, the values for the L length and the position of the probe feed were re-optimized separately for the L and W values determined with DE and PSO. This led to slight variations in the L-lengths and probe positions, resulting in a complete resonant and impedance match at 6.2 GHz. The results are shown in Tables 4 and 5, respectively. Figure 4 shows the frequency variation of the return loss S_{11} for the RPMA determined with IE3D with the patch size values of L = 14.12 mm and W = 11.10 mm highlighted in bold in Table 5. With this patch size, the antenna appears to have the best matching at f_r of 6.2 GHz compared to other patch sizes.

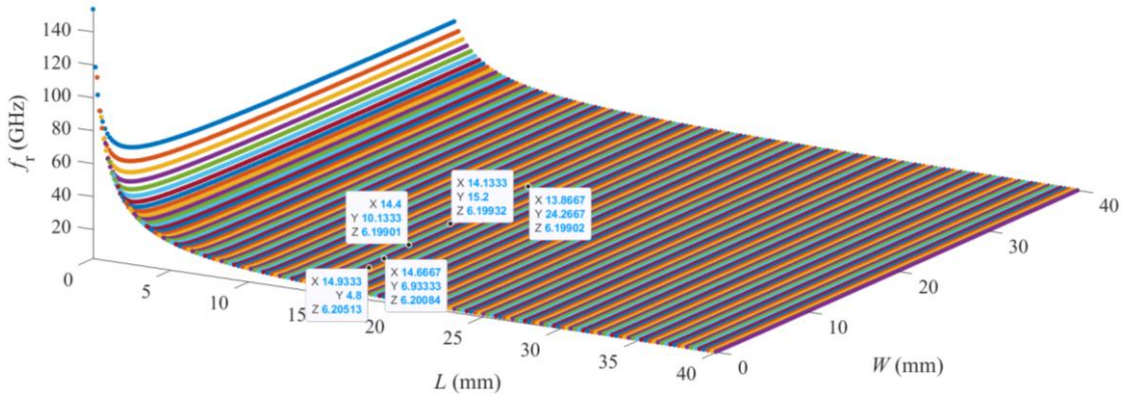

Fig. 3. Variation of f_r with respect to patch width W and patch length L for ε_r = 2.55 and h = 2 mm.

Table 2. Patch sizes (L and W) calculated with DE for f_r = 6.2 GHz, ε_r = 2.55, and h = 2 mm, and outputs obtained with IE3D using these dimensions, substrate values and x_{in} optimized by IE3D.

Inputs : f_r = 6.2 GHz, ε_r = 2.55, h = 2 mm					
Outputs Calculated by DE with specified search space		Outputs obtained by IE3D			
L (mm) (L_{min}, L_{max})	W (mm) (W_{min}, W_{max})	f_r (GHz)	BW (MHz)	S_{11} (dB)	x_{in} (mm) (optimized)
14.5 (14, 14.5)	8.75 (8, 9)	6.15	250	-18.84	4.81
14.22 (14, 14.5)	13.31 (13, 13.5)	6.16	324	-21.02	3.66
14.24 (10, 25)	12.89 (0, 20)	6.16	317	-20.92	3.78
14.36 (0, 20)	10.75 (0, 20)	6.16	284	-20.15	4.33
14.30 (0, 20)	11.63 (0, 20)	6.16	298	-20.79	4.11
14.21 (0, 20)	13.53 (0, 20)	6.16	328	-21.31	3.61
14.16 (0, 20)	14.51 (0, 20)	6.17	342	-22.76	3.38
14.18 (0, 20)	14.11 (0, 20)	6.17	335	-22.88	3.52
15 (15, 20)	4.48 (0, 20)	6.18	174	-21.87	6.07
14.10 (0, 20)	16.11 (0, 20)	6.18	360	-25.86	3.02
14.06 (0, 20)	17.18 (0, 20)	6.18	371	-28.00	2.73
14 (14, 20)	18.94 (0, 20)	6.19	385	-36.38	2.23
13.99 (0, 20)	**19.29 (0, 20)**	**6.2**	**387**	**-40.36**	**2.12**

Table 3. Patch sizes (L and W) calculated with PSO for f_r = 6.2 GHz, ε_r = 2.55, and h = 2 mm, and outputs obtained with IE3D using these dimensions, substrate values and x_{in} optimized by IE3D.

Inputs : f_r = 6.2 GHz, ε_r = 2.55, h = 2 mm					
Outputs Calculated by PSO with specified search space		Outputs obtained by IE3D			
L (mm) (L_{min}, L_{max})	W (mm) (W_{min}, W_{max})	f_r (GHz)	BW (MHz)	S_{11} (dB)	x_{in} (mm) (optimized)
14.5 (14, 14.5)	8.75 (8, 9)	6.15	250	-18.84	4.81
14.22 (14, 14.5)	13.31 (13, 13.5)	6.16	324	-21.02	3.66
14.24 (10, 25)	12.89 (0, 20)	6.16	317	-20.92	3.78
14.61 (0, 20)	7.48 (0, 20)	6.16	234	-18.84	5.16
14.79 (0, 20)	5.86 (0, 20)	6.16	204	-20.13	5.64
14.34 (0, 20)	11.10 (0, 20)	6.16	292	-20.40	4.23
14.83 (0, 20)	5.56 (0, 20)	6.17	196	-20.58	5.74
15	4.48	6.18	174	-21.87	6.07

(15, 20)	(0, 20)				
15.13 (0, 20)	3.82 (0, 20)	6.18	159	-24.79	6.30
15.21 (0, 20)	3.42 (0, 20)	6.18	143	-25.41	6.44
14 (14, 20)	18.94 (0, 20)	6.19	385	-36.38	2.23
13.99 (0, 20)	19.38 (0, 20)	6.2	385	-39.41	2.09
13.98 **(0, 20)**	**19.70** **(0, 20)**	**6.2**	**378**	**-41.26**	**2.08**

Table 4. L and x_{in} values optimized by IE3D for f_r = 6.2 GHz, ε_r = 2.55, h = 2 mm and fixed W values obtained by DE, and outputs obtained with IE3D by using these values

Inputs : f_r = 6.2 GHz, ε_r = 2.55, h = 2 mm					
The optimized values of L by using IE3D with fixed W values obtained by DE		The outputs obtained by IE3D			
L (mm) (optimized)	W (mm)	f_r (GHz)	BW (MHz)	S_{11} (dB)	x_{in} (mm) (optimized)
14.29	**8.75**	**6.2**	**237**	**-48.34**	**5.01**
14.06	13.31	6.2	312	-34.36	3.9
14.04	12.89	6.2	305	-40.13	4.03
14.15	10.75	6.2	271	-38.62	4.55
14.12	11.63	6.2	292	-39.39	4.3
14.03	13.53	6.2	312	-37.34	3.9
13.99	14.51	6.2	319	-36.03	3.66
14	14.11	6.2	326	-43.72	3.7
14.88	4.48	6.2	169	-31.79	6.14
13.97	16.11	6.2	346	-42.42	3.21
13.97	17.18	6.2	360	-43.62	2.89
13.96	18.94	6.2	380	-40.51	2.33
13.96	19.29	6.2	380	-43.69	2.19

Table 5. L and x_{in} values optimized by IE3D for f_r = 6.2 GHz, ε_r = 2.55, h = 2 mm and fixed W values obtained by PSO, and outputs obtained with IE3D by using these values.

Inputs : f_r = 6.2 GHz, ε_r = 2.55, h = 2 mm					
The optimized values of L by using IE3D with fixed W values obtained by PSO		The outputs obtained by IE3D			
L (mm) (optimized)	W (mm)	f_r (GHz)	BW (MHz)	S_{11} (dB)	x_{in} (mm) (optimized)
14.3	8.75	6.2	240	-42.55	5
14.02	13.31	6.2	305	-41.30	3.95
14.04	12.89	6.2	305	-41.25	4.04
14.43	7.48	6.2	215	-43.24	5.34
14.66	5.86	6.2	190	-45.98	5.75
14.12	**11.1**	**6.2**	**280**	**-50.28**	**4.43**
14.69	5.56	6.2	185	-42.52	5.81
14.9	4.48	6.2	165	-47.30	6.13
15.06	3.82	6.2	155	-43.32	6.33
15.16	3.42	6.2	145	-36.76	6.48
13.95	18.94	6.2	380	-43.23	2.35
13.99	19.38	6.2	390	-40.87	2.10
13.98	19.70	6.2	390	-45.41	2.01

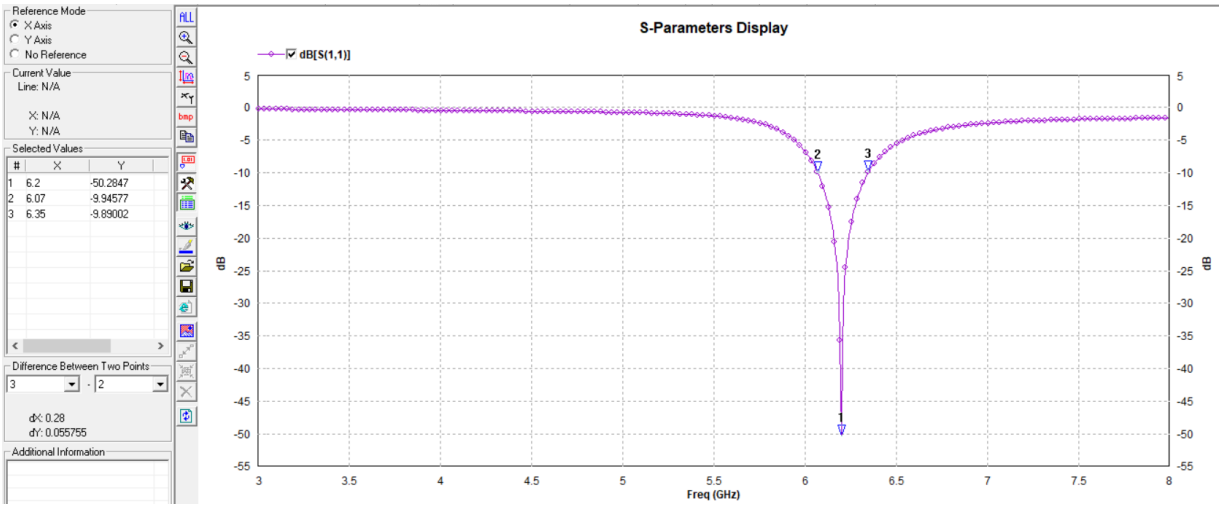

Fig. 4. The frequency variation of the return loss (S_{11} in dB) obtained with the IE3D program for the RPMA with patch size values of L = 14.12 mm and W = 11.1 mm.

The performances of DE and PSO were evaluated by running these algorithms 30 times in the same search space for L and W ((14, 14.5) mm and (8, 9) mm, respectively), resulting in identical values for L and W (14.5 mm and 8.75 mm, respectively). Figure 5 shows the convergence curves of the best solutions when each algorithm is run 30 times separately. It shows that DE and PSO reach the optimal value of zero at the 55^{th} and 64^{th} iteration, respectively. In other words, DE has a faster convergence speed than PSO. The boxplots of the data obtained from the 30 runs with DE and PSO are shown in Figure 6. This figure illustrates that PSO exhibits a zero interquartile range and a narrower interquartile range compared to DE, suggesting superior search stability. Additionally, PSO demonstrates no outliers across the 30 runs, whereas DE presents two outliers. The statistical data for 30 runs are shown in Table 6.

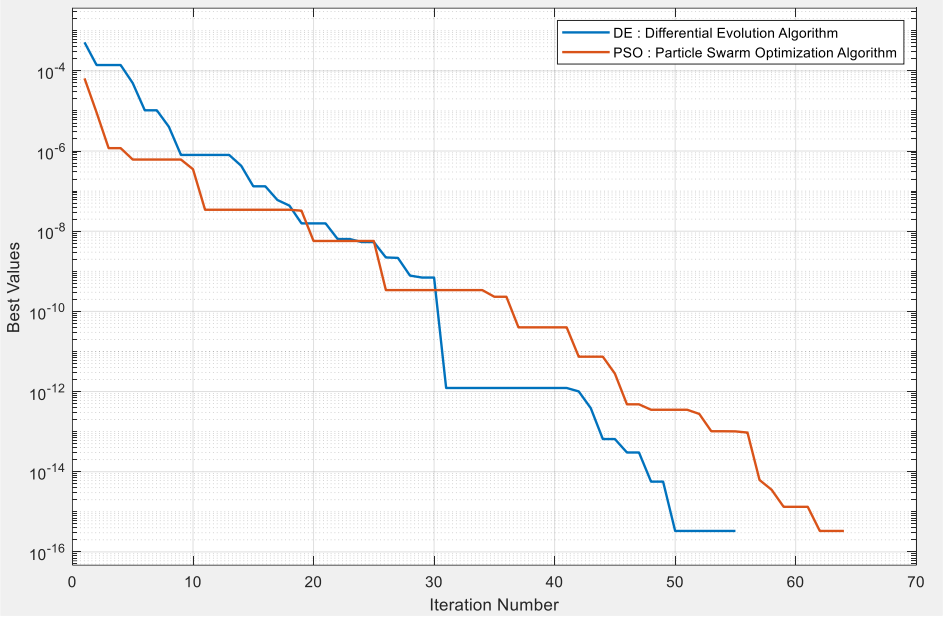

Fig. 5. Convergence curves of optimization algorithms for the best solution.

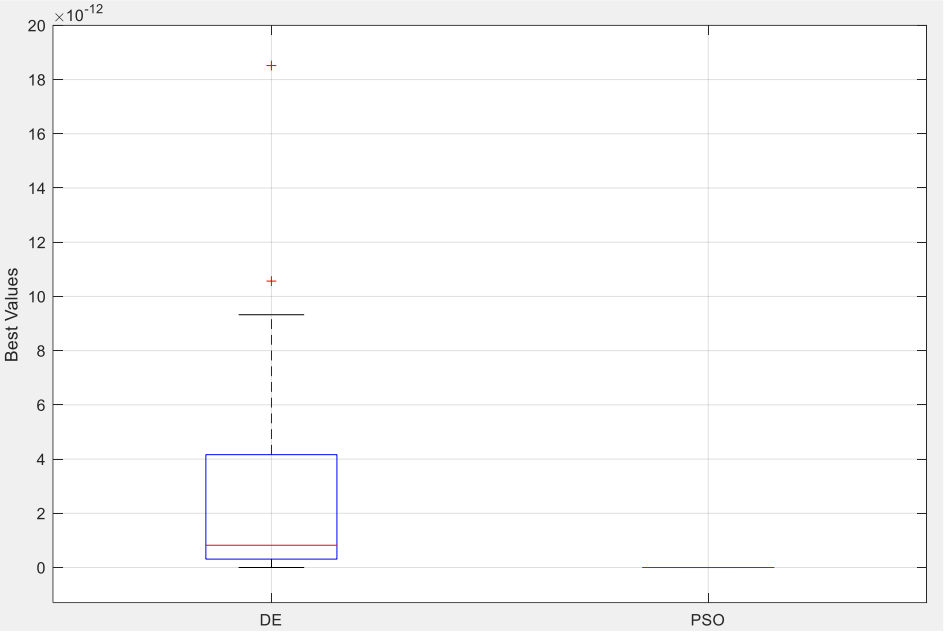

Fig. 6. Boxplots of optimization algorithms for 30 runs.

Table 6. Statistical values obtained from 30 runs.

Method	Best Solution	Mean Solution	Worst Solution	Standard Deviation	Average Time (sec)
DE	0	2.78×10^{-12}	1.85×10^{-11}	3.98×10^{-12}	0.12
PSO	0	0	0	0	0.09

To demonstrate the practical validity of the study, Table 7 compares the measured results from the literature for 33 different resonant frequencies with the results from (1) and the IE3D program. Here, the electrical thickness h/λ_d ranges from 0.0065 to 0.2284, where λ_d is the wavelength in the dielectric substrate. It can be seen that sufficient matching at f_r for values beyond an electrical thickness of 0.1814 cannot be achieved with IE3D. However, it can be seen that the results are relatively consistent for all f_r values obtained. Furthermore, with IE3D, both the lengths L or W and the position of the probe feed point can be easily adjusted to achieve a perfect match at the desired f_r. The deviations of the theoretical and simulated results of f_r of each antenna from the measured results are also shown in the table as Δf_{r1} and Δf_{r2}, respectively. The average absolute deviation of the theoretical results from the measured results is 8.64%, while the simulation results show a deviation of 1.63%. From this, we can conclude that the simulation study with IE3D shows a better agreement with the measured results than the results obtained with the theoretical expression from (1).

Table 7. Comparison of the resonant frequencies of some rectangular patch microstrip antennas experimentally realized in the literature with the results obtained with theoretical and IE3D methods.

Anten No	Physical Parameters				Meas. [19, 20]	(1)	Outputs obtained by IE3D				Δf_{r1}	Δf_{r2}	h/λ_d $\times10^{-2}$
	W (mm)	L (mm)	h (mm)	ε_r	f_r (GHz)	f_r (GHz)	f_r (GHz)	BW (MHz)	S_{11} (dB) at f_r	x_{in} (mm)			
1	8.50	12.90	0.17	2.22	7.74[19]	7.81	7.73	44.44	-28.82	4.78	-0.9	0.13	0.65
2	7.90	11.85	0.17	2.22	8.45[19]	8.50	8.41	48.15	-32.98	4.50	-0.59	0.47	0.71
3	20.00	25.00	0.79	2.22	3.97[19]	4	3.94	39.51	-17.91	8.95	-0.76	0.76	1.56
4	10.63	11.83	0.79	2.55	7.73[19]	7.77	7.64	153.09	-25.73	4	-0.52	1.16	3.25
5	18.10	19.60	1.57	2.33	4.805[19]	4.85	4.76	128.4	-19.52	6.06	-0.94	0.94	3.84
6	17.20	18.60	1.57	2.33	5.06[20]	5.09	5.01	143.21	-16.24	5.46	-0.59	0.99	4.04
7	15.00	16.21	1.63	2.55	5.6[19]	5.57	5.50	159.26	-12.89	4.26	0.54	1.79	4.86
8	12.70	13.50	1.63	2.55	6.56[19]	6.60	6.52	275.31	-21.8	3.78	-0.61	0.61	5.69
9	9.10	10.00	1.27	10.2	4.6[19]	4.68	4.52	39.51	-27.83	3.9	-1.74	1.74	6.22
10	13.37	14.12	2.00	2.55	6.2[19]	6.24	6.18	320.99	-27.47	3.8	-0.65	0.32	6.60
11	14.03	14.85	2.52	2.55	5.8[19]	5.83	5.81	367.90	-33.28	3.84	-0.52	-0.17	7.78
12	15.30	16.30	3.00	2.50	5.27[19]	5.32	5.32	372.84	-26.28	4.09	-0.95	-0.95	8.33
13	11.20	12.00	2.42	2.55	7.05[19]	7.09	7.12	496.3	-19.07	3.06	-0.57	-0.99	9.08
14	11.70	12.80	3.00	2.50	6.57[19]	6.59	6.65	560.5	-16.61	2.96	-0.3	-1.22	10.39
15	9.05	10.18	3.00	2.50	7.99[19]	8.02	8.32	416.05	-10.86	2.29	-0.38	-4.13	12.63
16	13.75	15.80	4.76	2.55	5.1[19]	5.12	5.33	345.68	-11.30	3.3	-0.39	-4.51	12.92
17	7.76	10.80	3.30	2.55	8[20]	7.56	8.18	928.4	-13.43	2	5.5	-2.25	14.05
18	9.87	14.50	4.50	2.55	6.07[20]	5.64	6.15	743.21	-13.52	2.57	7.08	-1.32	14.54
19	10.00	15.20	4.76	2.55	5.82[20]	5.38	5.88	691.36	-13.23	2.83	7.56	-1.03	14.75
20	7.90	12.55	4.00	2.55	7.134[20]	6.52	7.26	916.05	-13.09	2.1	8.61	-1.77	15.19
21	12.00	19.70	6.26	2.55	4.66[20]	4.16	4.67	617.28	-13.28	3.13	10.73	-0.21	15.53
22	8.14	14.40	4.76	2.55	6.38[20]	5.69	6.41	743.21	-12.15	2.58	10.82	-0.47	16.17

23	7.90	16.20	5.50	2.55	5.99[20]	5.09	5.91	683.95	-11.61	2.65	15.03	1.34	17.54
24	12.56	27.56	9.52	2.55	3.58[20]	3	3.54	320.99	-10.85	4.19	16.2	1.12	18.14
25	10.20	26.40	9.52	2.55	3.9[20]	3.15	3.81	–	-9.72	4.07	19.23	2.31	19.76
26	9.74	26.20	9.52	2.55	3.98[20]	3.18	3.98	–	-9.16	3.04	20.1	0	20.17
27	12.65	35.00	12.81	2.55	2.98[20]	2.38	2.90	–	-9.30	5.52	20.13	2.68	20.32
28	7.83	23.00	8.54	2.55	4.6[20]	3.63	4.47	–	-9.11	3.81	21.09	2.83	20.91
29	8.83	26.76	10.00	2.55	3.98[20]	3.12	3.86	–	-8.93	4.33	21.61	3.02	21.19
30	10.80	34.00	12.81	2.55	3.15[20]	2.46	3.05	–	-8.69	5.58	21.9	3.17	21.48
31	10.30	33.80	12.81	2.55	3.2[20]	2.48	3.1	–	-8.55	5.55	22.5	3.13	21.82
32	9.20	31.30	12.00	2.55	3.47[20]	2.69	3.36	–	-8.4	5.27	22.48	3.17	22.17
33	7.77	28.35	11.00	2.55	3.9[20]	2.98	3.78	–	-8.17	4.75	23.59	3.08	22.84

6. Conclusion

In this study, a novel approach representing alternative patch size solutions for predicting of specified resonant frequencies of conventional RPMAs was presented. DE and PSO optimization methods were used to determine the patch dimensions of RPMAs for a f_r of 6.2 GHz within specified search spaces. Thirteen alternative patch dimensions were identified for this f_r using DE and PSO separately. The accuracy of the proposed method was evaluated using the IE3D program, which showed consistent results. Furthermore, the performances of DE and PSO algorithms were compared when they achieved the same patch sizes (L = 14.5 mm and W = 8.75 mm) within the same search space (L_{min} = 14 mm, L_{max} = 14.5 mm, W_{min} = 8 mm, W_{max} = 9 mm) over 30 runs. PSO demonstrated greater stability compared to DE, although DE converged faster to the best cost than PSO. Both algorithms offered simple, accurate, and fast solutions. Finally, the practical validity of the theoretical and simulation approaches used in the study was evaluated by comparing their approximations with experimental results from the literature. It was found that for electrical thicknesses above 0.1814, sufficient impedance matching at f_r could not be achieved with IE3D. Theoretical results had an average absolute deviation of 8.64% from the measurement results, while the simulation results showed an average absolute deviation of 1.63% from the measurement results. The method proposed in this study shows promise for use and further improvement in other microwave circuits and antenna designs for wireless network applications. In the future studies, the performance of different optimization algorithms will be tested on defined or similar problems. Additionally, it is planned to assess the performance of antennas by fabricating them for various resonant frequencies and simulating them using software tools like CST and HFSS.

Acknowledgements

The author declares that he has no known competing financial interests or personal relationships that could have appeared to influence the work reported in this paper.

Author Contributions

B.H.: Conceptualization, methodology, software, data curation, writing-original draft preparation, visualization, investigation, supervision, validation, writing-reviewing and editing.

References

[1] C. A. Balanis, *Antenna theory: analysis and design*. John Wiley & Wons, 2016.
[2] R. Garg, P. Bhartia, I. Bahl, and A. Ittipiboon, *Microstrip antenna design handbook*. Artech House, Canton, MA, 2001.
[3] D. M. Pozar and D. H. Schaubert (Eds.), *Microstrip antennas—The analysis and design of microstrip antennas and arrays*. IEEE Press, New York, 1995.

[4] K. Carver and J. Mink, "Microstrip antenna technology," *IEEE Transactions on Antennas and Propagation*, vol. 29, no. 1, pp. 2-24, 1981. https://doi.org/10.1109/TAP.1981.1142523.
[5] B. Hiçdurmaz and F.G.Ömer, "Design and analysis of 28 GHz microstrip patch antenna for diferent type FR4 claddings," *Uludağ Üniversitesi Mühendislik Fakültesi Dergisi*, vol. 24, no. 2, pp. 265-288, 2019. https://doi.org/10.17482/uumfd.548410.
[6] I. J. Bahl and P. Bhartia, *Microstrip antennas*. Dedham, MA. Artech House, 1980.
[7] J. R. James, P. S. Hall, and C. Wood, *Microstrip antennas-theory and design*. London, UK: Peter Peregrinus, 1981.
[8] D. L. Sengupta, "Approximate expression for the resonant frequency of a rectangular patch antenna," *Electronics Letters*, vol. 20, no. 19, pp. 834-835, 1983. https://doi.org/10.1049/el:19830568.
[9] R. Garg and S. A. Long, "Resonant frequency of electrically thick rectangular microstrip antennas," *Electronics Letters*, vol. 21, no. 23, pp. 1149-1151, 1987. https://doi.org/10.1049/el:19870801.
[10] D. Karaboga, K. Guney, S. Sagiroglu, and M. Erler, "Neural computation of resonant frequency of electrically thin and thick rectangular microstrip antennas," *IEE Proceedings Microwave Antennas and Propagation*, vol. 146, no. 2, pp. 155-156, 1999. https://doi.org/10.1049/ip-map:19990136.
[11] Z. Wang, X. Li, S. Fang, and Y. Liu, "An accurate edge extension formula for calculating resonant frequency of electrically thin and thick rectangular patch antennas with and without air gaps," *IEEE Access*, vol. 4, pp. 2388-2397, 2016. https://doi.org/10.1109/ACCESS.2016.2565684.
[12] K. Guney, "A new edge extension expression for the resonant frequency of rectangular microstrip antennas with thin and thick substrates," *Journal of Communications Technology and Electronics*, vol. 49, no. 1, pp. 49-53, 2004.
[13] A. Akdagli, "An empirical expression for the edge extension in calculating resonant frequency of rectangular microstrip antennas with thin and thick substrates," *Journal of Electromagnetic Waves and Applications*, vol. 21, no. 9, pp. 1247-1255, 2007. https://doi.org/10.1163/156939307794731222.
[14] A. Akdagli, "A closed-form expression for the resonant frequency of rectangular microstrip antennas," *Microwave Optical Technology Letters*, vol. 49, no. 8, pp. 1848-1852, 2007. https://doi.org/10.1002/mop.22572.
[15] E. Chang, S. A. Long, and W. F. Richards, , "An experimental investigation of electrically thick rectangular microstrip antennas," *IEEE Transaction on Antennas and Propagation*, vol. 34, no. 6, pp. 767-772, 1986. https://doi.org/10.1109/TAP.1986.1143890.
[16] K. Guney, "A new edge extension expression for the resonant frequency of electrically thick rectangular microstrip antennas," *International Journal of Electronics*, vol. 75, no. 4, pp. 767-770, 1993. https://doi.org/10.1080/00207219308907154.
[17] I. Lee and A. V. Vorst, "Resonant-frequency calculation for electrically thick rectangular microstrip patch antennas using a dielectric-looded inhomogeneous cavity model," *Microwave Optical Technology Letters*, vol. 7, no. 15, pp. 704-708, 1994. https://doi.org/10.1002/mop.4650071509.
[18] M. Kara, "The resonant frequency of rectangular microstrip antenna elements with various substrate thicknesses," *Microwave Optical Technology Letters*, vol. 11, no 2, pp. 55-59, 1996. https://doi.org/10.1002/(SICI)1098-2760(19960205)11:2<55::AID-MOP1>3.0.CO;2-N.
[19] M. Kara, "Formulas for the computation of the physical properties of rectangular microstrip antenna elements with various substrate thicknesses," *Microwave Optical Technology Letters*, vol. 12, no. 4, pp. 234-239, 1996. https://doi.org/10.1002/(SICI)1098-2760(199607)12:4<234::AID-MOP15>3.0.CO;2-A.
[20] M. Kara, "Closed-form expressions for the resonant frequency of rectangular microstrip antenna elements with thick substrates," *Microwave Optical Technology Letters*, vol. 12, no. 3, pp. 131-136, 1996. https://doi.org/10.1002/(SICI)1098-2760(19960620)12:3<131::AID-MOP4>3.0.CO;2-I.
[21] M. Kara, "Empirical formulas for the computation of the physical properties of rectangular microstrip antenna elements with thick substrates," *Microwave Optical Technology Letters*, vol. 14, no. 2, pp. 115-121. 1997. https://doi.org/10.1002/(SICI)1098-2760(19970205)14:2<115::AID-MOP12>3.0.CO;2-A.
[22] M. Kara, "Design considerations for rectangular microstrip antenna elements with various substrate thicknesses," *Microwave Optical Technology Letters*, vol. 19, no. 2, pp. 111-121, 1998. https://doi.org/10.1002/(SICI)1098-2760(19981005)19:2<111::AID-MOP8>3.0.CO;2-J.
[23] K. P. Ray and G. Kumar, "Determination of the resonant frequency of microstrip antennas," *Microwave Optical Technology Letters*, vol. 23, no. 2, pp. 114-117, 1999. https://doi.org/10.1002/(SICI)1098-2760(19991020)23:2<114::AID-MOP15>3.0.CO;2-G.
[24] S. S. Pattnaik, B. Khuntia, D. C. Panda, D. K. Neog, and S. Devi, "Calculation of optimized parameters of rectangular microstrip patch antenna using genetic algorithm," *Microwave Optical Technology Letters*, vol. 37, no. 6, pp. 431-433, 2003. https://doi.org/10.1002/mop.10940.
[25] K. Guney, "Simple and accurate formulas for the physical dimensions of rectangular microstrip antennas with thin and thick substrates," *Microwave Optical Technology Letters*, vol. 44, no. 3, pp. 257-259, 2005. https://doi.org/10.1002/mop.20603.
[26] A. Akdagli, "CAD formulas for patch dimensions of rectangular microstrip antennas with various substrate thicknesses," *Microwave Optical Technology Letters*, vol. 49, no. 9, pp. 2197-2201, 2007. https://doi.org/10.1002/mop.22679.
[27] A. E. Yilmaz and M. Kuzuoglu, "Calculation of optimized parameters of rectangular microstrip patch antenna using particle swarm optimization," *Microwave Optical Technology Letters*, vol. 49, no. 12, pp. 2905-2907, 2007. https://doi.org/10.1002/mop.22918.
[28] R. W. Dearnley and A. R. F. Barel, "A comparison of models to determine the resonant frequencies of a rectangular microstrip antenna," *IEEE Transactions on Antennas and Propagation*, vol. 37, no. 1, pp. 114–118, 1989. https://doi.org/10.1109/8.192173.
[29] L. Merad, F. T. Bendimerad, and S. M. Meriah, "Design and resonant frequency calculation of rectangular microstrip antennas," *International Journal of Numerical Modelling: Electronic Networks, Devices and Fields*, vol. 24, no. 2, pp. 144-153, 2011. https://doi.org/10.1002/jnm.767.
[30] D. Ustun, F. Toktas, and A. Toktas, "An optimized surrogate model using differential evolution algorithm for computing parameters of antennas," *International Journal of Numerical Modelling: Electronic Networks, Devices and Fields*, vol. 35, no. 2, e2951, 2022. https://doi.org/10.1002/jnm.2951.
[31] T. Yu-Bo, Z. Su-Ling, and L. Jing-Yi, "Modeling resonant frequency of microstrip antenna based on neural network ensemble," *International Journal of Numerical Modelling: Electronic Networks, Devices and Fields*, vol. 24, no. 1, pp. 78-88, 2011. https://doi.org/10.1002/jnm.761.

[32] E. O. Hammerstad, "Equations for microstrip circuits design," *Proceeding of the Fifth European Microwave Conference*, Hamburg, 1975, pp. 268–272. https://doi.org/10.1109/euma.1975.332206.
[33] E. Suganya, T. A. J. M. Pushpa, and T. Prabhu, "Advancements in patch antenna design for Sub-6 GHz 5G smartphone application: a comprehensive review." *Wireless Personal Communications*, vol. 137, no. 4, pp. 2217-2252, 2024. https://doi.org/10.1007/s11277-024-11484-7.
[34] A. S. A. Gaid, M. A. M. Ali, A. Saif, and W. A. A. Mohammed, "Design and analysis of a low profile, high gain rectangular microstrip patch antenna for 28 GHz applications," *Cogent Engineering*, 11: 2322827, 2024. https://doi.org/10.1080/23311916.2024.2322827.
[35] K. Sharma and G. P. Pandey, "Efficient modelling of compact microstrip antenna using machine learning," *AEU-International Journal of Electronics and Communications*, 135:153739, 2021. https://doi.org/10.1016/j.aeue.2021.153739.
[36] A. Farahbakhsh and D. Zarifi, "Miniaturization of patch antennas by curved edges," *AEU-International Journal of Electronics and Communications*, 117:153125, 2020. https://doi.org/10.1016/j.aeue.2020.153125.
[37] A. A. Elijah and M. Mokayef, "Miniature microstrip antenna for IoT application," *Materials Today: Proceedings*, vol. 29, pp. 43-47, 2020. https://doi.org/10.1016/j.matpr.2020.05.678.
[38] O. W. Ata, M. Salamin, and K. Abusabha, "Double U-slot rectangular patch antenna for multiband applications," *Computers and Electrical Engineering*, 84:106608, 2020. https://doi.org/10.1016/j.compeleceng.2020.106608.
[39] C. A. Diniz, L. A. Costa, O. M. da Costa Pereira-Filho, and F. J. da Silva Moreira, "Fringing field correction for spherical–rectangular microstrip antennas," *AEU-International Journal of Electronics and Communications*, 127:153447, 2020. https://doi.org/10.1016/j.aeue.2020.153447.
[40] F. C. Acıkaya and B. S. Yıldırım, "A dual-band microstrip patch antenna for 2.45/5-GHz WLAN applications," *AEU-International Journal of Electronics and Communications*, 141:153957, 2021. https://doi.org/10.1016/j.aeue.2021.153957.
[41] O. Ossa-Molina and F. López-Giraldo, "A simple model to compute the characteristic parameters of a slotted rectangular microstrip patch antenna," *Electronics*, vol. 11, no. 1, p. 129, 2022. https://doi.org/10.3390/electronics11010129.
[42] H. Yiğit and K. Karayahşi, "A novel model-based technique to improve design processes for microstrip antennas," *AEU-International Journal of Electronics and Communications*, 162:154570, 2023. https://doi.org/10.1016/j.aeue.2023.154570.
[43] A. J. Kulkarni and P. Siarry, *Handbook of AI-based metaheuristics*, CRC Press, 2022.
[44] R. Storn and K. Price, "Differential evolution - a simple and efficient heuristic for global optimization over continuous spaces," *Journal of Global Optimization*, vol. 11, pp. 341-359, 1997. https://doi.org/10.1023/A:1008202821328.
[45] K. Guney and D. Karaboga, "New narrow aperture dimension expressions obtained by using a differential evolution algorithm for optimum gain pyramidal horns," *Journal of Electromagnetic Waves and Applications*, vol. 18, no. 3, pp. 321-339, 2004. https://doi.org/10.1163/156939304323085694.
[46] X. F. Luo, A. Qing, and C. K. Lee, "Application of the differential evolution strategy to the design of frequency-selective surfaces," *International Journal of RF and Microwave Computer-Aided Engineering*, vol. 15, no. 2, pp. 173-180, 2005. https://doi.org/10.1002/mmce.20065.
[47] A. Akdagli and M. E. Yuksel, "Application of differential evolution algorithm to the modeling of laser diode nonlinearity in a radio-over-fiber network," *Microwave Optical Technology Letters*, vol. 48, no. 6, pp. 1130-1133, 2006. https://doi.org/10.1002/mop.21560.
[48] C. Yildiz, A. Akdagli, and M. Turkmen, "Simple and accurate synthesis formulas obtained by using a differential evolution algorithm for coplanar striplines," *Microwave Optical Technology Letters*, vol. 48, no. 6, pp. 1133-1137, 2006. https://doi.org/10.1002/mop.21559.
[49] P. Rocca, G. Oliveri, and A. Massa, "Differential evolution as applied to electromagnetics," *IEEE Antennas and Propagation Magazine*, vol. 53, no. 1, pp. 38-49, 2011. https://doi.org/10.1109/MAP.2011.5773566.
[50] B. Hiçdurmaz, H. Temurtaş, S. E. Karlık, and G. Yılmaz, "A novel method degrading the combined effect of FWM and ASE noise in WDM systems containing in-line optical amplifiers," *Optik*, vol. 124, no. 19, pp. 4064-4071, 2013. https://doi.org/10.1016/j.ijleo.2012.12.071.
[51] J. S. Muñoz-Reina, M. G. Villarreal-Cervantes, and L. G. Corona-Ramírez, "Integrated design of a lower limb rehabilitation mechanism using differential evolution," *Computers and Electrical Engineering*, vol. 92:107103, 2021. https://doi.org/10.1016/j.compeleceng.2021.107103.
[52] J. Kennedy and R. Eberhart, "Particle swarm optimization," In *Proceedings of ICNN'95-International Conference on Neural Networks*, 1995, pp. 1942-1948. https://doi.org/10.1109/ICNN.1995.488968.
[53] Y. Shi and R. Eberhart, "A modified particle swarm optimizer," In *1998 IEEE International Conference on Evolutionary Computation Proceedings. IEEE World Congress on Computational Intelligence (Cat. No. 98TH8360)*, 1998, pp. 69-73. https://doi.org/10.1109/ICEC.1998.699146.
[54] Y. Shi and R. C. Eberhart, "Empirical study of particle swarm optimization," In *Proceedings of the 1999 Congress on Evolutionary Computation-CEC99 (Cat. No. 99TH8406)*, 1999, pp. 1945-1950. https://doi.org/10.1109/CEC.1999.785511.
[55] J. Robinson and Y. Rahmat-Samii, "Particle swarm optimization in electromagnetics," *IEEE Transactions on Antennas and Propagation*, vol. 52, no. 2, pp. 397-407, 2004. https://doi.org/10.1109/TAP.2004.823969.
[56] N. Jin and Y. Rahmat-Samii, "Particle swarm optimization for antenna designs in engineering electromagnetics," *Journal of Artificial Evolution and Applications*, 2008. https://doi.org/10.1155/2008/728929.
[57] W. C. Weng and C. T. Choi, "Optimization comparison between Taguchi's method and PSO by design of a CPW slot antenna," In *2009 IEEE Antennas and Propagation Society International Symposium*, 2009, pp. 1-4. https://doi.org/10.1109/APS.2009.5171497.
[58] D. Wang, D. Tan, and L. Liu, "Particle swarm optimization algorithm: an overview," *Soft Computing*, vol. 22, pp. 387-408, 2018. https://doi.org/10.1007/s00500-016-2474-6.
[59] T. M. Shami, A. A. El-Saleh, M. Alswaitti, and Q. Al-Tashi, "Summakieh, M. A., Mirjalili, S. Particle swarm optimization: A comprehensive survey," *IEEE Access*, vol. 10, pp. 10031-10061, 2022. https://doi.org/10.1109/ACCESS.2022.3142859.
[60] X. Xiang, X. Yan, C. Gao, S. Zhu, M. Xi, and H. Gao, "A circle chaos random search strategy particle swarm optimization with its application," *Computers and Electrical Engineering*, 102:108219, 2022. https://doi.org/10.1016/j.compeleceng.2022.108219.

[61] B. Hiçdurmaz, "Determination of the optimal input channel powers using particle swarm optimization algorithm in a WDM system with In-Line optical amplifiers," *Optical Fiber Technology*, 77:103254, 2023. https://doi.org/10.1016/j.yofte.2023.103254.